Published in final edited form as:
Nano Lett. 2013 September 11; 13(9): 4294–4298. doi:10.1021/nl402054w.

In Vivo Whole Animal Fluorescence Imaging of a Microparticle-Based Oral Vaccine Containing ($CuInSe_xS_{2-x}$)/ZnS Core/Shell Quantum Dots

Matthew G. Panthani, **Tarik A. Khan**, **Dariya K. Reid**, **Daniel J. Hellebusch**, **Michael R. Rasch**, **Jennifer A. Maynard***, and **Brian A. Korgel***
Department of Chemical Engineering, Texas Materials Institute, and Center for Nano- and Molecular Science and Technology, The University of Texas at Austin, Austin, TX 78712

Abstract

Zinc sulfide-coated copper indium sulfur selenide ($CuInSe_xS_{2-x}$/ZnS core/shell) nanocrystals were synthesized with size-tunable red to near infrared (NIR) fluorescence with high quantum yield (40%) in water. These nanocrystals were tested as an imaging agent to track a microparticle-based oral vaccine administered to mice. Poly(lactic-*co*-glycolic acid) (PLGA) microparticle-encapsulated $CuInSe_xSe_{2-x}$/ZnS quantum dots were orally administered to mice and were found to provide a distinct visible fluorescent marker in the gastrointestinal tract of living mice.

Keywords

Quantum dots; $CuInSe_2$; $CuInS_2$; near infrared; in vivo imaging; bioimaging; photoluminescence

Semiconductor nanocrystal quantum dots can exhibit bright and stable fluorescence with color that can be tuned over a wide wavelength range by changing size and composition, making them suitable as fluorescent bioimaging probes.[1–4] For biological imaging, nanocrystals with near infrared (NIR) optical signal are of particular interest because there is a spectral window through tissue and water between 650 and 900 nm.[5,6] Fluorescent quantum dots can also be photoexcited over a very wide range of wavelengths, enabling multispectral imaging.[7, 8] In contrast, there are few bright molecular fluorophores with excitation or emission wavelengths in these ranges.[9] One other advantage of fluorescent quantum dots over molecular dyes is that they can be photoexcited over a very wide range of wavelengths, which is important for multispectral imaging.[7,8] Bioimaging using quantum dots has been demonstrated a number of times, typically administered using intravenous routes.[10,11]

Here, we report the synthesis of ZnS-coated copper indium sulfide-selenide ($CuInSe_xS_{2-x}$) quantum dots with bright fluorescence with quantum yields in water of up to 40% and their use as fluorescent contrast agents for *in vivo* imaging of orally administered microparticles. Room-temperature photoluminescence (PL) is rarely observed from bulk $CuInSe_xS_{2-x}$ or other ternary I-III-VI compounds due to nonradiative recombination at defects,[12] but quantum dots of several related materials have been made with bright room temperature PL,

*Corresponding authors: (T) +1-512-471-9188, (F): +1-512-471-7060, maynard@che.utexas.edu; (T) +1-512-471-5633, (F) +1-512-471-7060k korgel@che.utexas.edu.

SUPPORTING INFORMATION
Experimental details, analysis of *in vivo* fluorescence imaging data, and photoluminescence spectra. This material is available free of charge via the Internet at http://pubs.acs.org.

including $Cu(In_xGa_{1-x})Se_2$13, $CuInS_2$, $CuInSe_2$14, $Cu_2ZnSnS_4$15 and I-III-VI ordered vacancy compound nanocrystals,[16] and ZnS-coated $CuInS_2$.[17] The peak emission wavelength of the core/shell $CuInSe_xS_{2-x}$/ZnS quantum dots could be tuned by size through a range of red/NIR wavelengths suitable for *in vivo* biological imaging. Furthermore, the $CuInSe_xS_{2-x}$/ZnS quantum dots do not contain toxic elements (such as Cd, Pb, Hg, or As) like most other NIR-emitting nanocrystals, such as Pb chalcogenides,[18,19] CdTe,[20] InAs,[21] and Cd_3As_2.[22] In addition to bioimaging, these quantum dots could be attractive for optoelectronic applications such as solar cells and light-emitting diodes.[23] As proof-of-principle *in vivo* imaging, $CuInSe_xS_{2-x}$/ZnS quantum dots were used to track the movement of orally-administered poly(lactic-co-glycolic acid) (PLGA) microparticles in mice. The quantum dots were encapsulated in PLGA microparticles functionalized with the bacterial protein invasin to facilitate mucosal vaccine delivery. Using *in vivo* whole animal fluorescence imaging, the microparticles were observed to accumulate in deep tissue within the gastrointestinal tract of the mouse. This experiment demonstrates the feasibility of fluorescent nanocrystal quantum dots for *in vivo* imaging of orally administered particles.

$CuInSe_xS_{2-x}$ nanocrystals were synthesized by arrested precipitation in octadecene at 220°C with Cu(acac), $In(acac)_3$ (2.5 g), tributylphosphine selenide (TBP:Se) and dodecanethiol as capping ligand and sulfur source. (See Supporting Information for details.) Tuan and coworkers recently synthesized $CuInSe_xS_2$ nanocrystals in gram scale quantities using elemental Se and S as chalcogen sources,[24] however those nanocrystals were too large (>10 nm) to be luminescent. We find that using a combination of dodecanethiol and tertiary phosphine selenides as chalcogen sources allows for slow growth necessary to control the size in the 1 to 3 nm diameter range. It was, however, also not possible using this method to effectively make nanocrystals in the larger size range (>3 nm diameter). McDaniel, et al.[25] used a similar synthesis approach to $CuInSe_xS_{2-x}$ quantum dots for use in solar cells, but did not show the ability to control the nanocrystal size.

Figure 1 shows TEM images of $CuInSe_xS_2$ nanocrystals isolated at different times during the reaction. The nanocrystals become progressively larger, increasing from 1.1 nm after 2 min to 3.1 nm in diameter after 60 min. Longer reaction times did not lead to significantly larger nanocrystals. Figure 2 shows X-ray diffraction (XRD) of the nanocrystals made with 750 nm peak emission wavelength. XRD (Figure 2) is consistent with sphalerite or chalcopyrite $CuInSe_xS_2$ and no other phases are present in the reaction product. Chalcopyrite (tetragonal) $CuInSe_2$ ($CuInS_2$) should exhibit diffraction peaks at ~17(18)° and ~35(37)° corresponding to the (101) and (211) lattice planes. The sphalerite (111) peak (chalcopyrite (112) peak) lies at $2\Theta=27.1°$ (d=3.29 Å), in between the (112) peak positions for chalcopyrite copper indium selenide and copper indium sulfide (JCPDS #97-006-892, 082-1702), indicating that the nanocrystals are an S-Se alloy. The lattice spacing measured in the high resolution TEM image in Figure 1C is 3.25 Å, consistent with (112) lattice planes of chalcopyrite $CuInSe_xS_2$. A core/shell structure, or gradient in S-Se composition within the nanocrystals cannot be ruled out, however, given that the diffraction peaks are relatively broad. Using Vegard's law to estimate the composition based on the lattice spacing determined from the (112) XRD peak, the S:Se composition is 1.1:0.9. The Cu:In:S:Se composition determined by EDS was 1.0:1.0:1.3:0.7. EDS provides an overestimate of the S composition in the nanocrystal core due to the presence of the thiol capping ligands in the sample. The S:Se composition of nanocrystals made at longer reaction times measured by EDS did not vary significantly with reaction time. Nanocrystals synthesized at lower temperatures, at 200°C and less, were richer in Se, indicating that dodecanethiol is less reactive as a sulfur source than TBP:Se as a Se source at lower temperatures. Nanocrystals synthesized at these lower temperatures also exhibited substantially lower PL quantum yields. At reaction temperatures higher than 240°C, it was not possible to maintain narrow size distributions and obtain sizes in the range needed for

quantum confinement and luminescence. The reaction product would begin to precipitate within within a few minutes of injecting the reactants.

Figure 3 shows absorbance and PL spectra of the $CuInSe_xS_{2-x}$ nanocrystals. Nanocrystals isolated immediately after TBP:Se injection (0 min) exhibited an absorbance shoulder at approximately 380 nm and weak PL at 610 nm (QY < 0.01%). As the reaction proceeds and the $CuInSe_xS_2$ nanocrystals grow, the absorbance shoulder and PL shift to longer wavelength, consistent with quantum confinement. Bulk $CuInSe_xS_2$ with the same composition calculated from the $CuInSe_xS_2$ composition determined by EDS has band gap of about 1.2 eV (1030 nm). Between 5 and 15 min, the PL spectra appear to have a slightly bimodal emission, similar to what has previously been observed in $CuInS_2$ quantum dots and attributed to defect-related emission.[17, 26] Overcoating with ZnS resulted in a significant increase of PL quantum yield to 40% and a slight redshift in the peak position of ~20 nm (Supporting Information, S1). The ZnS overcoated nanocrystals retained their bright fluorescence for several months even when stored in air.

$CuInSe_xS_2$/ZnS quantum dots were integrated into a microparticle-based oral vaccine system. Previous work has shown that the *Y. pseudotuberculosis*–derived protein invasin targets intestinal M cells by binding the $\alpha_5\beta_1$ integrin with high specificity and affinity. M cells are present in the gastrointestinal tract, occurring at a frequency of ~1 in 10^7 enterocytes.[27] They represent the first line of intestinal immune responses, sampling material present in the gut lumen and delivering it to underlying lymphocytes. These cells in turn mediate mucosal immune responses, for instance, to combat bacterial or viral pathogens.[25, 26] Since access to lymphocytes is a major limitation in oral delivery of subunit vaccines, targeting M cells has emerged as a general strategy for oral vaccine delivery. [30–34] Wild-type invasion binds the $\alpha_5\beta_1$ integrin with high affinity, but a single amino acid substitution, replacement of an aspartic acid residue at position 911 with an alanine (D911A), completely abrogates binding.[35] Both variants are readily expressed and purified in high yield from a heterologous *E. coli* expression system comprised of the extracellular D1–D5 invasin domains fused downstream of the soluble carrier protein, maltose binding protein (MBP), hereafter referred to as invasin. The fluorescent $CuInSe_xS_2$/ZnS quantum dots were used to monitor transport of an invasin-functionalized vaccine delivery system in living mice.

Fluorescent $CuInSe_xS_2$ nanocrystals were encapsulated in poly (lactic-co-glycolic) acid microparticles formed by a microemulsion method (see Supporting information for experimental details). Figure 4 shows a SEM and fluorescence microscopy images of the micropoarticles containing $CuInSe_xS_2$ nanocrystals. The microparticles are fluorescent and somewhat polydisperse, ranging in diameter from 500 nm to 2 μm. Figure 4e shows a photograph of a microparticle dispersion illuminated by a UV lamp. To assess *in vivo* microparticle transport and localization, they were decorated with either wild-type or the non-binding D911A invasin variant via EDC-NHS conjugation. A schematic illustrating the experimental process is shown in Figure 5.

The mice were placed on an alfalfa free diet to reduce intestinal autofluorescence and fasted for three hours prior to dosing to reduce mouse-to-mouse variability. Invasin functionalized PLGA microparticles (15 mg) encapsulating the $CuInSe_xS_2$ nanocrystals ($InvaCuInSe_xS_{2-x}$) were orally gavaged to mice (three per group) and imaged, using a non-invasive Caliper Life Sciences IVIS Spectrum In Vivo Imaging System, to track the time-dependent fluorescence retention in the gastrointestinal tract. The mice were then anesthetized by isoflurane inhalation and imaged, while maintaining anesthesia. Images were collected at 15 min, 18 hr, and at the terminal time point, two days after dosage. This study was performed with approval by the Institutional Animal Care and Use Committee at the University of Texas at

Austin (protocol #AUP-2009-00086) in compliance with guidelines from the Office of Laboratory Animal Welfare. Figure 6 shows whole-animal fluorescence images of mice fed InvaCuInSe$_x$S$_{2-x}$.

Quantum dot fluorescence was clearly visible in the whole-animal images and identified the location of the microparticles *in vivo*. At 15 minutes, any material orally gavaged would be primarily found in the stomach, as the exponential decay constant of stomach emptying in the mouse is 72 min.[36] The fluorescence signal in figures 6(a) and (e) is located where the stomach should be located. At 18 and 45 hours, the majority of ingested material that is not mucoadhesive or transported across the intestinal wall is expected to be excreted. Figure 6(h) shows the fluorescence signal is restricted to the cecum and the colon. In mice, M cells are found along the gastrointestinal tract in Peyer's patches in the distal small intestine, isolated lymphoid follicles, cecal patches, and colonic patches.[37, 38] The bulk of the invasin-conjugated particles appear to be retained in this region. Quantitative analysis was performed by integrating the fluorescence intensity over a region of interest encompassing the entire abdomen using multiple filter sets (Figure 7). For images with weaker signals (18h, 45h, intestines), the images were spectrally unmixed using Living Image 4.0 to distinguish tissue autofluorescence from nanocrystal fluorescence (supporting information for details). Comparisons between samples groups show a slight trend in increased intestinal retention at 48 h for the wild-type invasin group. Factors such as protease degradation of invasion during gastrointestinal tract transit may reduce the differences between these groups.

Conclusions

Colloidal ZnS-coated CuInSe$_x$S$_{2-x}$ quantum dots with size-dependent, bright PL were synthesized. The ZnS shell increased the PL quantum yield of the CuInSe$_x$S$_2$ nanocrystals from around 10% to 40% and stabilized the PL in aqueous media. These nanocrystals are attractive for medical imaging since they emit red/NIR light and do not contain toxic heavy metals. As a proof-of-principle, CuInSe$_x$S$_2$ nanocrystals were loaded into invasion-functionalized PLGA microparticles and were observed in deep tissue within the gastrointestinal tract by i*n vivo* whole animal fluorescence imaging. The CuInSe$_x$S$_2$ nanocrystals are promising new biocompatible diagnostic agents.

Supplementary Material

Refer to Web version on PubMed Central for supplementary material.

Acknowledgments

Funding was provided by the Robert A. Welch Foundation (grant no. F-1464 to BAK and F-1767 to JAM), the Gates Foundation Grand Challenges (to JAM) and the National Institutes of Health (Grant No. R01 CA132032 to BAK). We thank Ralph Isberg (Tufts University) for the pRI203 plasmid, and Krishnendu Roy and Keith Johnston (UT Austin) for use of their facilities to make the PLGA particles.

References

1. Michalet X, Pinaud FF, Bentolila LA, Tsay JM, Doose S, Li JJ, Sundaresan G, Wu AM, Gambhir SS, Weiss S. Science. 2005; 307:538–544. [PubMed: 15681376]
2. Medintz IL, Uyeda HT, Goldman ER, Mattoussi H. Nature Mater. 2005; 4:435–446. [PubMed: 15928695]
3. Hessel CM, Rasch MR, Hueso JL, Goodfellow BW, Akhavan VA, Puvanakrishnan P, Tunnel JW, Korgel BA. Small. 2010; 6:2026–2034. [PubMed: 20818646]

4. Kairdolf BA, Smith AM, Stokes TD, Wang MD, Young AN, Nie S. Ann Rev Anal Chem. 2013; 610.1146/annurev-anchem-060908-155136
5. Farokhzad OC, Langer R. Adv Drug Delivery Rev. 2006; 58:1456–1459.
6. Madelung, O. Semiconductors other than Group IV Elements and III-V Compounds. New York: 1992.
7. Resch-Genger U, Grabolle M, Cavaliere-Jaricot S, Nitschke R, Nann T. Nature Methods. 2008; 5:763–775. [PubMed: 18756197]
8. Fountaine TJ, Wincovitch SM, Geho DH, Garfield SH, Pittaluga S. Mod Pathol. 2006; 19:1181–1191. [PubMed: 16778828]
9. Frangioni JV. Curr Op Chem Bio. 2003; 7:626–634.
10. Ballou B, Lagerholm BC, Ernst LA, Bruchez MP, Waggoner AS. Bioconjugate chemistry. 2003; 15(1):79–86. [PubMed: 14733586]
11. Pons T, Pic E, Lequeux N, Cassette E, Bezdetnaya L, Guillemin F, Marchal F, Dubertret B. ACS Nano. 2010; 4(5):2531–2538. [PubMed: 20387796]
12. Chichibu S. Appl Phys Lett. 1997; 70:1840–1842.
13. Panthani MG, Akhavan V, Goodfellow B, Schmidtke JP, Dunn L, Dodabalapur A, Barbara PF, Korgel BA. J Am Chem Soc. 2008; 130:16770–16777. [PubMed: 19049468]
14. Zhong H, Wang Z, Bovero E, Lu Z, van Veggel FCJM, Scholes GD. J Phys Chem C. 2011; 115:12396–12402.
15. Steinhagen C, Panthani MG, Akhavan V, Goodfellow B, Koo B, Korgel BA. J Am Chem Soc. 2009; 131:12554–12555. [PubMed: 19685876]
16. Allen PM, Bawendi MG. J Am Chem Soc. 2008; 130:9240–9241. [PubMed: 18582061]
17. Li L, Daou TJ, Texier I, Kim Chi TT, Liem NQ, Reiss P. Chem Mater. 2009; 21:2422–2429.
18. Harbold JM, Du H, Krauss TD, Cho KS, Murray CB, Wise FW. Phys Rev B. 2005; 72:195312.
19. Murphy JE, Beard MC, Norman AG, Ahrenkiel SP, Johnson JC, Yu P, Micic OI, Ellingson RJ, Nozik AJ. J Am Chem Soc. 2006; 128:3241–3247. [PubMed: 16522105]
20. Peng ZA, Peng X. J Am Chem Soc. 2000; 123:183–184. [PubMed: 11273619]
21. Guzelian AA, Banin U, Kadavanich AV, Peng X, Alivisatos AP. Appl Phys Lett. 1996; 69:1432–1434.
22. Harris DK, Allen PM, Han HS, Walker BJ, Lee J, Bawendi MG. J Am Chem Soc. 2011; 133:4676–9. [PubMed: 21388210]
23. Panthani MG, Korgel BA. Ann Rev Chem Biomol Eng. 2012; 3:287–311. [PubMed: 22468605]
24. Chiang MY, Chang SH, Chen CY, Yuan FW, Tuan HY. J Phys Chem C. 2011; 115:1592–1599.
25. McDaniel H, Fuke N, Pietryga JM, Klimov VI. J Phys Chem Lett. 2013; 4:355–361.
26. Zhong H, Zhou Y, Ye M, He Y, Ye J, He C, Yang C, Li Y. Chem Mater. 2008; 20:6434–6443.
27. Tyrer PC, Ruth Foxwell A, Kyd JM, Otczyk DC, Cripps AW. Vaccine. 2007; 25:3204–3209. [PubMed: 17276559]
28. Clark MA, Hirst BH, Jepson MA. Infect Immun. 1998; 66:1237–1243. [PubMed: 9488419]
29. Hussain N, Florence AT. Pharmaceutical Res. 1998; 15:153–156.
30. Palumbo RN, Wang C. Curr Drug Delivery. 2006; 3:47–53.
31. Shukla A, Katare OP, Singh B, Vyas SP. Int J Pharmaceutics. 2010; 385:47–52.
32. Nochi T, Yuki Y, Matsumura A, Mejima M, Terahara K, Kim DY, Fukuyama S, Iwatsuki-Horimoto K, Kawaoka Y, Kohda T, Kozaki S, Igarashi O, Kiyono H. J Exp Med. 2007; 204:2789–2796. [PubMed: 17984304]
33. KuoLee R, Chen W. Exp Op Drug Delivery. 2008; 5:693–702.
34. Fievez V, Plapied L, des Rieux A, Pourcelle V, Freichels H, Wascotte V, Vanderhaeghen M-L, Jerôme C, Vanderplasschen A, Marchand-Brynaert J, Schneider Y-J, Préat V. Eur J Pharmaceutics and Biopharmaceutics. 2009; 73:16–24.
35. Leong JM, Morrissey PE, Marra A, Isberg RR. EMBO J. 1995; 14:422–431. [PubMed: 7532130]
36. Schwarz R, Kaspar A, Seelig J, Kunnecke B. Magnetic Resonance in Medicine. 2002; 48:255–261. [PubMed: 12210933]

37. Hase K, Kawano K, Nochi T, Pontes GS, Fukuda S, Ebisawa M, Kadokura K, Tobe T, Fujimura Y, Kawano S, Yabashi A, Waguri S, Nakato G, Kimura S, Murakami T, Iimura M, Hamura K, Fukuoka SI, Lowe AW, Itoh K, Kiyono H, Ohno H. Nature. 2009; 462:226–U101. [PubMed: 19907495]

38. McConnell EL, Basit AW, Murdan S. J Pharmacy and Pharmacology. 2008; 60:63–70.

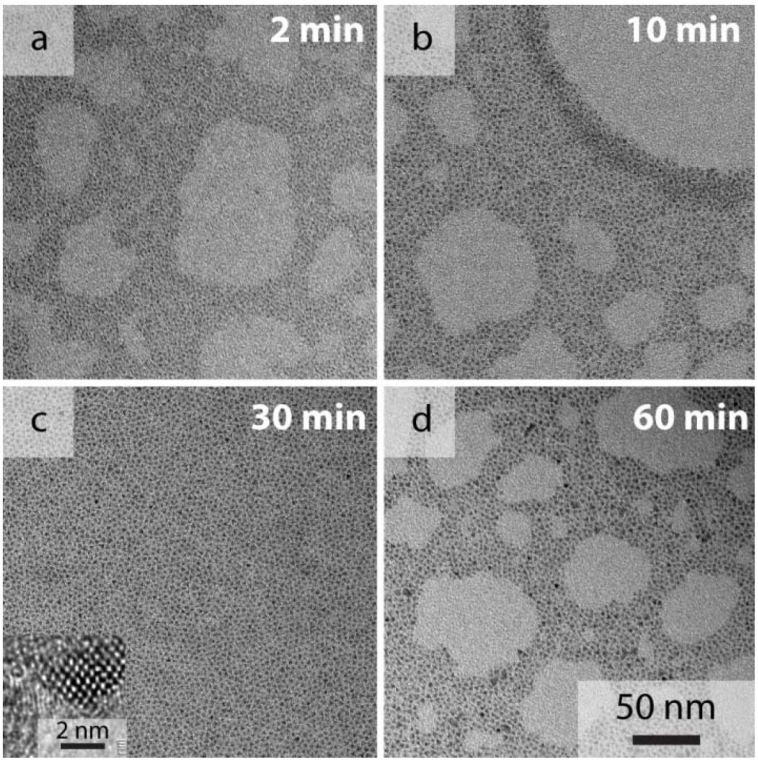

Figure 1.
TEM of $CuInSe_xS_2$ nanocrystals isolated at different times after reactant injection: (a) 2 min (1.1±0.3 nm), (b) 10 min (2.4±0.5), (c) 30 min (2.9±0.5), and (d) 1 hr (3.1±0.3). Inset in (c): High resolution TEM image of a $CuInSe_xS_2$ nanocrystal.

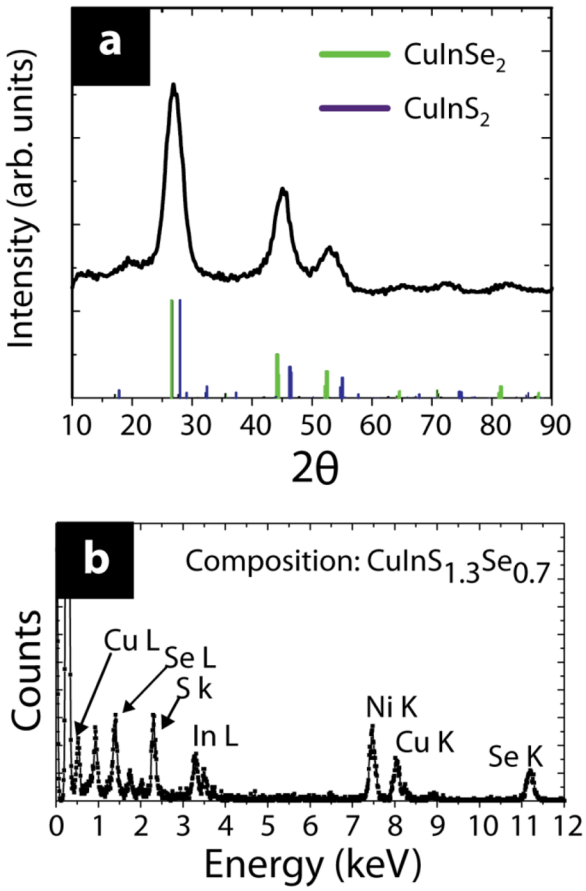

Figure 2.

(A) XRD and (B) EDS of $CuInSe_xS_{2-x}$ nanocrystals with emission at 750 nm (2.9 nm diameter). Reference patterns are provided in (A) for $CuInSe_2$ (green, JCPDS #97-006-892) and $CuInS_2$ (purple, JCPDS #082-1702).

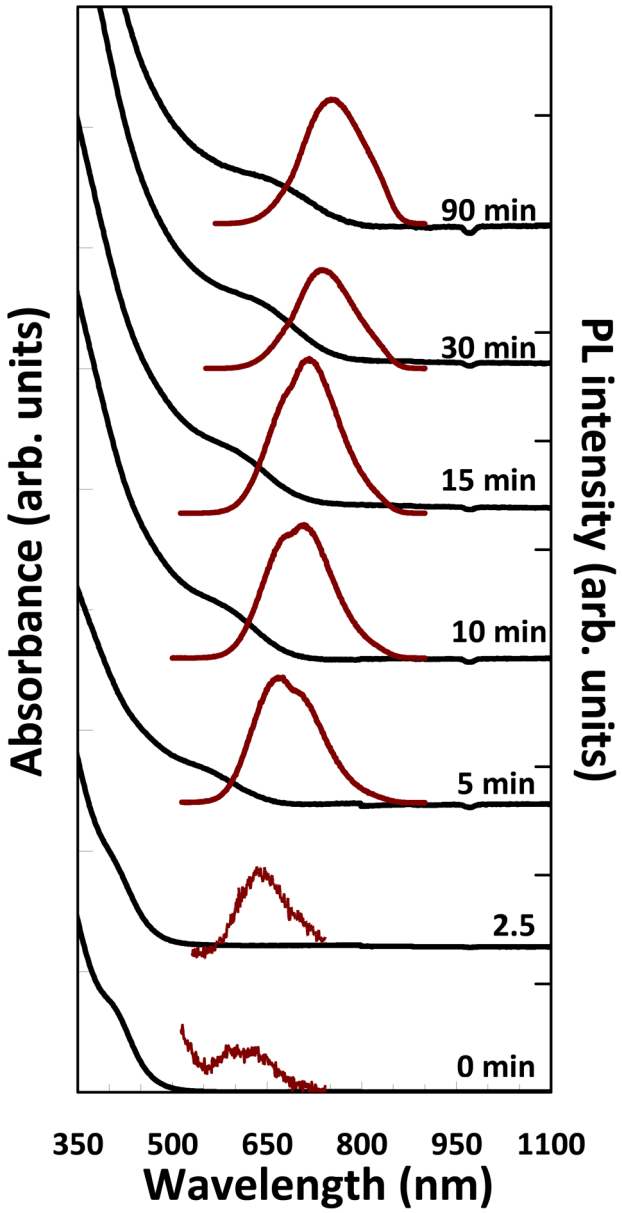

Figure 3.

Room temperature absorbance (black) and PL (λ_{exc}=400 nm) (red) spectra of uncoated $CuInSe_xS_2$ nanocrystals isolated at various times after reactant injection. The nanocrystals were dispersed in toluene.

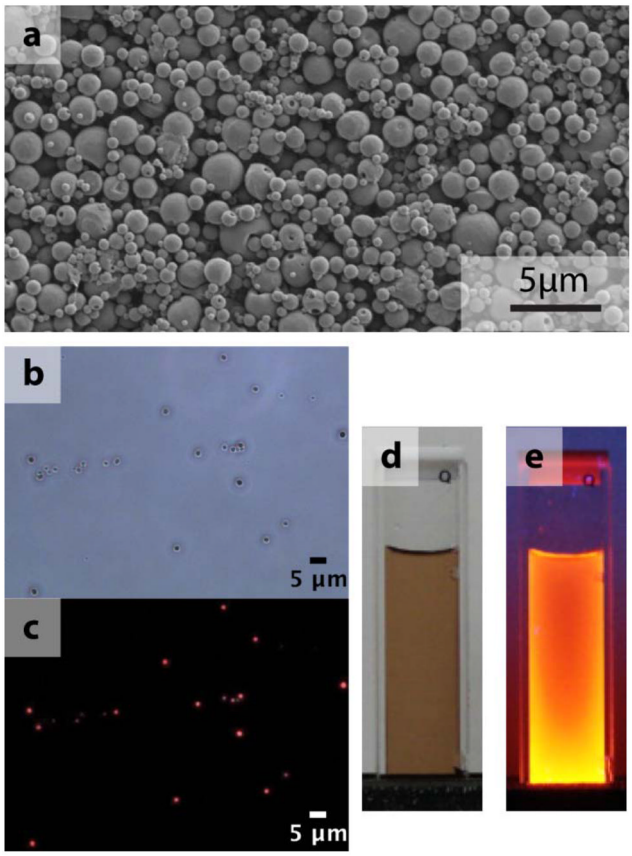

Figure 4.
(a) SEM image of a collection of InvaCuInSe$_x$S$_{2-x}$ particles, (b) an optical microscope image in bright field and (c) a corresponding fluorescence image (excitation 480 – 550 nm, emission >590 nm). (d) Photographs show the CuInSe$_x$S$_2$-nanocrystals dispersed in toluene in room light and (e) under UV exposure.

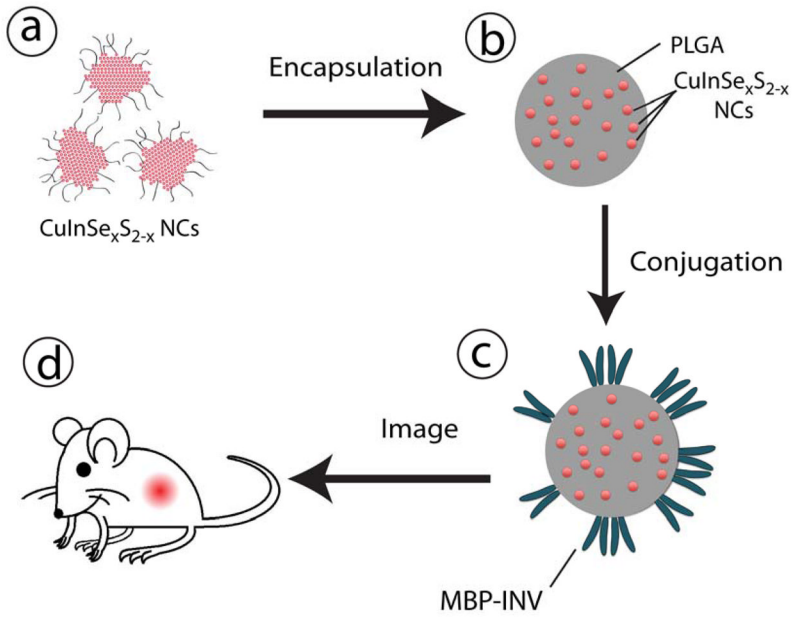

Figure 5.

Illustration of the experimental procedure. (a) $CuInSe_xS_2$-/ZnS quantum dots (NCs) dispersed in dichloromethane (DCM) are (b) encapsulated in PLGA microspheres, prior to (c) conjugation with wild-type invasin or non-binding variant D911A. (d) After intragastric gavage, *in vivo* fluorescence is monitored.

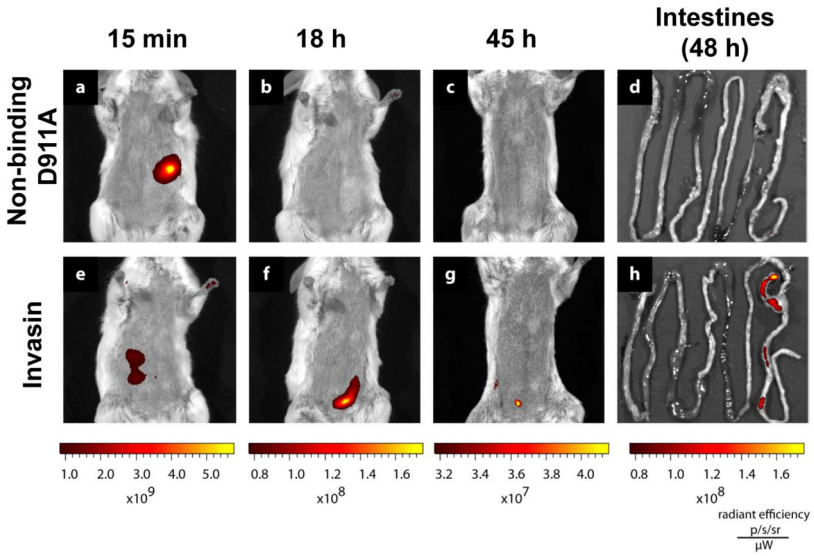

Figure 6.

Representative *in-vivo* fluorescence images tracking the same subjects at 15 min (a,e), 18 h (b,f), 45h (c,g) after oral gavage and the intestines after dissection at 48h (d,h). Mice (n= 3) were administered 15 mg InvaCuInSe$_x$S$_{2-x}$ microparticles conjugated with (e-h) wild type invasin or (a-d) the non-binding D911A variant.

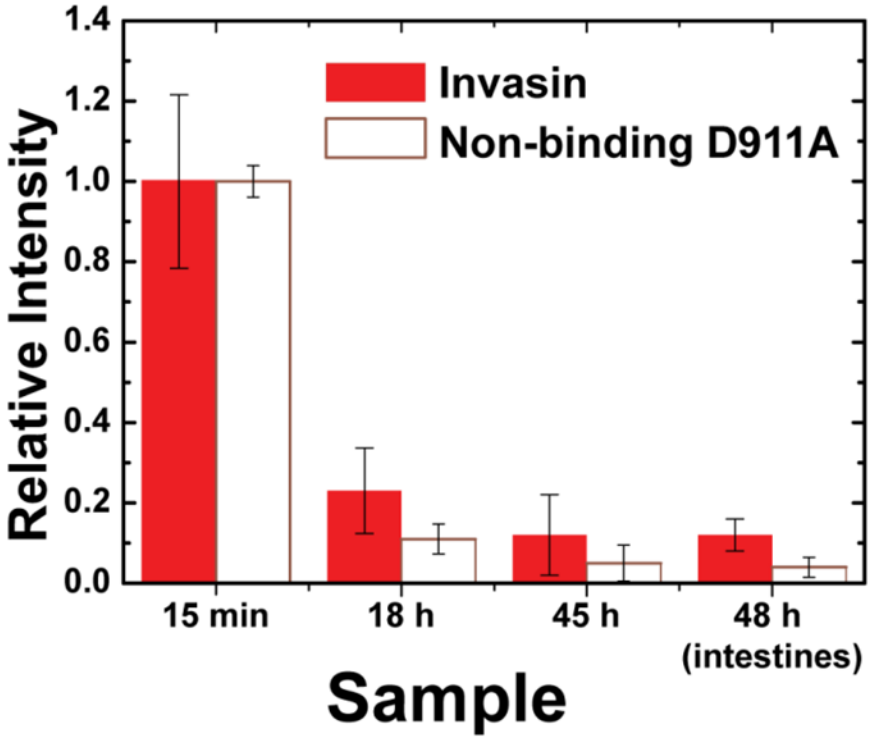

Figure 7.
Comparison of fluorescence signal from the nanocrystals at 15 min, 18 h, 45 h in vivo, and the intestines at 48 hours post-mortem. Error bars correspond to the standard deviation of measurements of individual mice for each sample group (wild-type n=3 and non-binding D911A n=2).